

Electronic Supplementary Information (ESI)

Hydrothermal treatment: an effective method to improve the catalytic activity of Pt/ZSM-5 catalyst for benzene total oxidation

Yunchong Wang,^{ab} Kaixuan Fu,^{ab} Haolong Huang,^{ab} Cangpeng Shan,^{ab} Yanfei Zheng,^{ab}

Rui Han,^{*ab} Qingling Liu^{*ab}

a. Tianjin Key Lab of Indoor Air Environmental Quality Control, School of

Environmental Science and Technology, Tianjin University, Tianjin, 300350, China

b. State Key Laboratory of Engines, School of mechanical engineering, Tianjin

University, Tianjin, 300350, China

* Correspondence: liuql@tju.edu.cn; Tel.:18522057634

hanr@tju.edu.cn; Tel.:18946119396

Experimental details

Chemicals and materials

$\text{H}_2\text{PtCl}_6 \cdot 6\text{H}_2\text{O}$ was purchased from Tianjin Chemart Chemical Technology Co. Ltd. ZSM-5 was purchased from Nankai Catalyst Company. All chemicals were used without any further purification.

Synthesis of Pt/ZSM-5

Platinum was loaded onto ZSM-5 by impregnation method. First, 0.531 mL of H_2PtCl_6 aqueous solution (19.3 mmol/L) and 1.199 mL deionized water were mixed well. Then the above solution was poured into 1 g ZSM-5 with stirring. After aging for 12 h, the sample was dried for 12 h at 110 °C and calcined in muffle at 550 °C for 5 h. The obtained catalyst was named as Pt/ZSM-5 with a theoretical Pt content of 0.2 wt.%. Without special statement, the $\text{SiO}_2/\text{Al}_2\text{O}_3$ ratio of ZSM-5 is 21

Hydrothermal treatment

Taking Pt/ZSM-5 (400-2h) as an example, the detailed steps are as follows. First, 0.11 g Pt/ZSM-5 was placed into a quartz tube reactor (6 mm i.d. × 500 mm length). Pure N_2 and O_2 (the ratio of $\text{N}_2/\text{O}_2 = 79:21$) were introduced in a total flow of 100 mL/min. Once the reactor was heated to 400 °C, the water vapor was fed by bubbling N_2 into the deionized water at 60 °C (the content of H_2O was about 10 vol.%). After the hydrothermal treatment lasted 2 h, pure N_2 and O_2 were introduced again for another 2 h at 400 °C to make the sample dry. Hydrothermally treated samples were marked as

Pt/ZSM-5 (x-yh), where x and y represented the treatment temperature and durations, respectively.

Catalytic activity tests

The catalytic activity tests were carried out in a quartz tube reactor (8 mm i.d. × 400 mm length). 1000 ppm of benzene (acetone or toluene) balanced by N₂ and O₂ was introduced into fixed bed reactor in a total flow of 51 mL/min, which resulted in the reaction gas containing 800 ppm VOCs, 21% O₂ and 79% N₂. 0.1 g of sample (40-60 mesh) was used in each test, and the space velocity (WHSV) of catalytic oxidation was 30000 mL/(g·h). The quartz tube reactor was heated from 120 °C to 260 °C using a resistance furnace. A thermocouple located in the middle of the reactor was used to measure the temperature of reactor. The VOCs gas and reaction products were online detected by a gas chromatograph (GC-9790II, FuLi) with two FID detectors. One was used for testing VOCs, and the other was for CO and CO₂.

The long-term stability and water resistance test was carried out at 160 °C for 50 h. The water vapor is generated by the N₂ bubbling in deionized water and the water content is regulated by controlling the temperature of the deionized water. In this work, 5 vol%. or 10 vol%. H₂O was obtained by controlling the temperature of water at 60 °C or 75 °C.

The calculations of VOCs conversion, CO₂ yield and turnover frequency (TOF) are described in the supplementary information.

Catalysts characterization

X-ray diffraction (XRD) patterns were collected by using Rigaku MiniFlex600 diffractometer with Cu K α radiation at 40 kV and 200 mA. The patterns were measured from 5 to 60° at a scanning rate of 10 °/min.

N₂ adsorption-desorption measurements were carried out on a physisorption analyzer (ASAP 2020 PLUS HD88, Micromeritics, USA) at -196 °C. The surface area and average pore volume was calculated using the Brunauer-Emmett-Teller (BET) method, and the pore size distribution was calculated using the density functional theory (DFT) method. The samples were degassed at 300 °C for 5 h under vacuum before testing.

The actual metal contents of Pt/ZSM-5, Pt/ZSM-5 (100-2h) and Pt/ZSM-5 (400-2h) were determined by Inductively Coupled Plasma Optical Emission Spectrometer (ICP-OES) technique (Agilent 725 ES).

The FT-IR spectrum were performed on a FT-IR spectrophotometer (Bruker TENSOR II) with the wavenumber range of 4000-600 cm⁻¹.

The morphologies were obtained by transmission electron microscope (TEM; JEM-F200, JEOL) and high-angle angular dark field scanning transmission electron microscopy (HAADF-STEM; JEM-F200, JEOL). The lattice fringe was measured by high resolution transmission electron microscope (HRTEM; JEM-F200, JEOL). The elements distribution was acquired by energy-dispersive X-ray spectroscopy (EDS, JED-2300T, JEOL).

CO Diffuse reflectance Fourier-transform infrared spectroscopy (DRIFTS) was performed on Nicolet IS20 (Thermo Fisher) with a MCT detector in the range of 4000-

400 cm^{-1} with a resolution of 4 cm^{-1} and 64 acquisition scans. Before adsorption, 20 mg sample was pretreated in N_2 (20 mL/min) at 300 °C for 60 min. After the sample was cooled down to room temperature (RT) and purged in N_2 for 30 min, the background was collected in N_2 . The sample was exposed to 1 vol.% CO/N_2 at flow rate of 20 mL/min for 45 min to reach the CO saturation coverage. Then N_2 was introduced to remove the gaseous CO and the spectra was recorded simultaneously.

NH_3 DRIFTS was performed on Nicolet IS20 (Thermo Fisher) with a MCT detector in the range of 4000-400 cm^{-1} with a resolution of 4 cm^{-1} and 64 acquisition scans. Before adsorption, 30 mg sample was pretreated in N_2 (30 mL/min) at 300 °C for 60 min. After the sample was cooled down to room temperature (RT) and purged in N_2 for 30 min, the background was collected in N_2 . The sample was exposed to 10 vol.% NH_3/N_2 at flow rate of 30 mL/min for 60 min to reach the NH_3 saturation coverage. Then N_2 was introduced to remove the gaseous NH_3 and the spectra was recorded simultaneously.

H_2O DRIFTS was performed on Nicolet IS20 (Thermo Fisher) with a MCT detector in the range of 4000-400 cm^{-1} with a resolution of 4 cm^{-1} and 64 acquisition scans. Before adsorption, 30 mg Pt/ZSM-5 catalyst was pretreated in N_2 (30 mL/min) at 500 °C for 60 min. Then, the sample was cooled down to target temperature (400 °C or 100 °C) and purged in mixed dry gas for 1 h (30 mL/min). The background was collected in mixed dry gas, and then the sample was exposed to mixed gas with 10 vol.% H_2O at flow rate of 30 mL/min. At the same time, the spectra was started to be recorded.

After 2 h hydrothermal treatment, the wet gas was transferred into dry gas (79 vol.%N₂ and 21 vol.%O₂) again for another 1 h.

X-ray photoelectron spectroscopy (XPS) experiment was carried out on ESCALAB Xi+ instrument (Thermo Fisher). Binding energy of all the elements was calibrated relative to the carbon impurity with a C 1s at 284.8 eV.

Hydrogen temperature programmed reduction (H₂-TPR) was performed on a BSD-Chem C200 (Beishide, China), with a TCD detector cooled by liquid nitrogen. 100 mg sample was pretreated in Ar (30 mL/min) at 300 °C for 2h. After cooling to 50 °C, the reduction was carried out under an atmosphere of H₂/Ar (30 mL/min). The temperature was raised from 30 °C to 800 °C at a heating rate of 10 °C/min.

Ammonia temperature programmed desorption (NH₃-TPD) was performed on a BSD-Chem C200 (Beishide, China), with a TCD detector cooled by liquid nitrogen. 100 mg sample was pretreated in He (30 mL/min) at 300 °C for 2h. After cooling to 50 °C, 10% NH₃/He was purged for 1 h (30 mL/min). The desorption was carried out under an atmosphere of He (30 mL/min). The temperature was raised from 30 °C to 800 °C at a heating rate of 10 °C/min.

CO chemisorption was carried out on a BSD-Chem C200 (Beishide, China), with a TCD detector. 100 mg sample was pretreated in He (30 mL/min) at 200 °C for 2h and cool down to 50 °C. After the sample was purged in He (30 mL/min) at 50 °C for 30 min, 1 vol% CO/He was introduced. The program stopped after the difference between the two adjacent peak areas is less than 0.1%. Details of Pt dispersion calculation can be found in **Calculations**.

In-situ Diffuse reflectance Fourier-transform infrared spectroscopy (DRIFTS) was performed on Nicolet IS20 (Thermo Fisher) with a MCT detector cooled by liquid nitrogen. 20 mg sample was pretreated in N₂ (20 mL/min) at 200 °C for 60 min and cooled down to 50 °C. After the sample was purged in N₂ (20 mL/min) for 30 min, the background was collected in N₂. Then 1000 ppm benzene, 21 vol% O₂ and N₂ (at a total flow rate of 15 mL/min) was introduced, and the spectra was recorded simultaneously. The same operation was carried out in the absence of oxygen. To investigate the possible reaction pathway of benzene over different catalysts, the temperature was increased from 100 °C to 180 °C in the presence of oxygen and the spectra was recorded at each temperature point.

Calculations

The conversion of benzene was calculated as:

$$\text{Benzene conversion (\%)} = \frac{[\text{Benzene}]_{\text{in}} - [\text{Benzene}]_{\text{out}}}{[\text{Benzene}]_{\text{in}}} \times 100\% \quad (1)$$

$$\text{CO}_2 \text{ yield (\%)} = \frac{[\text{CO}_2]_{\text{out}}}{[\text{Benzene}]_{\text{in}}} \times 100\% \quad (2)$$

where [Benzene]_{in} and [Benzene]_{out} are the benzene concentration in the inlet and outlet gas, respectively.

where [CO₂]_{out} are the outlet CO₂ concentration.

The calculation of Pt dispersion is based on the fact that CO is linearly adsorbed on Pt and it was obtained by the following formula:

$$D_M = \frac{a \times Q_{\text{total}}/22.4}{1000 \times (m \times \omega/M)}$$

(3)

where D_M is the Pt dispersion (%); a is the stoichiometric coefficient of metal atoms and adsorbate CO; Q_{total} is the total volume of CO adsorbed by the catalyst (cm^3); m is the mass of the catalyst (g); ω is the loading content of Pt (%); M is the molar weight of Pt ($\text{g}\cdot\text{mol}^{-1}$).

For calculating turnover frequency (TOF), which was defined as moles of acetone destructed per second per mole surface Pt sites. The SV was 30000 $\text{mL}/(\text{g}\cdot\text{h})$, and the reaction temperature was 140 °C. The TOF was calculated by the following formula:

$$TOF = \frac{r \times M_{pt}}{D_M \times x} \quad (4)$$

where r is the reaction rate of benzene ($\text{mol}\cdot\text{g}_{\text{cat}}^{-1}\cdot\text{s}^{-1}$), M_{Pt} is the molar weight of Pt ($195.05 \text{ g}\cdot\text{mol}^{-1}$), x is the Pt loading content, and D_M is the dispersion of Pt which is estimated by the CO chemisorption.

Table S1. Catalytic performance of benzene over a series of low Pt loading catalysts

Table S2. Physical properties of catalysts

Table S3. XPS results, Pt dispersion and TOF of catalysts

Figure S1. Acetone (a) and toluene (b) conversion curves over Pt/ZSM-5-21 and Pt/ZSM-5-21 (400-2h); benzene conversion curves over Pt/ZSM-5 and Pt/ZSM-5 (400-2h) with (c) 50 or (d) 85 SiO₂/Al₂O₃.

Figure S2. (a) Cycle stability tests over Pt/ZSM-5 (400-2h) catalyst; and (b) effect of WHSV over Pt/ZSM-5 (400-2h) catalyst.

Figure S3. The EDS mapping images of (a) Pt/ZSM-5, (b) Pt/ZSM-5 (100-2h) and (c) Pt/ZSM-5 (400-2h).

Figure S4. The Pt particle distribution of (a) Pt/ZSM-5, (b) Pt/ZSM-5 (100-2h) and (c) Pt/ZSM-5 (400-2h).

Figure S5. The XRD patterns of ZSM-5, Pt/ZSM-5 and Pt/ZSM-5 with different hydrothermal treatment.

Figure S6. The N₂ adsorption-desorption curve and pore diameter distribution of (a) Pt/ZSM-5, (b) Pt/ZSM-5 (100-2h), and (c) Pt/ZSM-5 (400-2h).

Figure S7. (a) Pt 4f and (b) O 1s XPS spectra of Pt/ZSM-5, Pt/ZSM-5 (100-2h) and Pt/ZSM-5 (400-2h).

Figure S8. The FT-IR spectrum of Pt/ZSM-5, Pt/ZSM-5 (100-2h) and Pt/ZSM-5 (400-2h).

Figure S9. A possible schematic of the destruction of bridging OH groups over Pt/ZSM-5 (400-2h)

Figure S10. Time-dependent CO DRIFT spectrum of (a) Pt/ZSM-5, (b) Pt/ZSM-5 (100-2h) and (c) Pt/ZSM-5 (400-2h) when purging with N₂; (d) CO DRIFT spectra of Pt/ZSM-5, Pt/ZSM-5 (100-2h) and Pt/ZSM-5 (400-2h) after N₂ purging.

Figure S11. Benzene conversion curves over ZSM-5 and in the absence of catalyst.

Figure S12. TOF values of Pt/ZSM-5, Pt/ZSM-5 (100-2h) and Pt/ZSM-5 (400-2h) at 140 °C.

Figure S13. The H₂-TPR patterns of Pt/ZSM-5, Pt/ZSM-5 (100-2h) and Pt/ZSM-5 (400-2h).

Figure S14. The NH₃-TPD patterns of Pt/ZSM-5, Pt/ZSM-5 (100-2h) and Pt/ZSM-5 (400-2h).

Figure S15. In-situ DRIFT spectrum of benzene adsorption over (a) Pt/ZSM-5 and (b) Pt/ZSM-5 (400-2h) at 50 °C.

Figure S16. Temperature-dependent in-situ DRIFT spectrum of benzene oxidation over (a) Pt/ZSM-5 and (b) Pt/ZSM-5 (400-2h).

Table S1 Catalytic performance of benzene over a series of low Pt loading catalysts

Sample	Pt content ^a (%)	WHSV mL/(g·h)	T ₉₀ (°C)	Benzene content (ppm)	references
Pt/ZSM-5	0.199	30000	179	800	this work
Pt/ZSM-5 (100-2h)	0.203	30000	172	800	this work
Pt/ZSM-5 (400-2h)	0.205	30000	158	800	this work
Pt ₁ /OMS-2	0.0383	20000	190	1000	1
Pt _{NP} /OMS-2	0.09	20000	206	1000	1
Pt/Al ₂ O ₃	0.43	40000	170	1000	2
Pt/ZSM-5	0.50	60000	160	1000	3
Pt/TS-1	0.20	60000	160	1000	4
Pt@Z5	0.20	20000	178	1000	5
Pt/10Ce-10V/ γ - Al ₂ O ₃	0.30	20000	235	1000	6
Pt/CeTi-EFD	0.50	15000	150	1000	7

^a The Pt content in this work was determined by ICP-OES

Table S1 listed the catalytic performance of catalysts synthesized in this work and a range of reported low-loaded Pt-based catalysts. Comparing with reported catalysts, Pt/ZSM-5 (400-2h) showed high catalytic activity for benzene oxidation. This result also demonstrated that hydrothermal treatment significantly improved the catalytic activity of Pt/ZSM-5.

Table S2 Physical properties of catalysts

Catalyst	$S_{\text{BET}}^{\text{a}}$ (m ² /g)	$S_{\text{micro}}^{\text{b}}$ (m ² /g)	$S_{\text{external}}^{\text{b}}$ (m ² /g)	$V_{\text{pore}}^{\text{c}}$ (cm ³ /g)	$D_{\text{pore}}^{\text{d}}$ (nm)
Pt/ZSM-5	303.1	213.7	89.4	0.22	2.98
Pt/ZSM-5 (100-2h)	283.8	206.5	77.3	0.21	2.99
Pt/ZSM-5 (400-2h)	317.9	228.4	89.4	0.23	2.90

^a Surface area by Brunauer-Emmett-Teller (BET) method

^b Micropore and external surface areas by the t-plot method

^c Total pore volumes of $P/P_0 = 0.95$

^d Average pore diameter ($4 V/A$ by BET)

Table S3 XPS results, Pt dispersion and TOF of catalysts

Samples	Pt ⁰ /(Pt ⁰ + Pt ⁴⁺ + Pt ²⁺) ^a (mol·mol ⁻¹)	O _{ads} /(O _{latt} + O _{ads}) ^a (mol·mol ⁻¹)	Pt dispersion ^b (%)	TOF of Pt sites ^c (10 ⁻³ ·s ⁻¹)
Pt/ZSM-5	0.322	0.939	44.66	1.47
Pt/ZSM-5 (100-2h)	0.377	0.954	37.50	3.89
Pt/ZSM-5 (400-2h)	0.447	0.975	16.99	21.69

^a Calculated by XPS integral area

^b Calculated by CO chemisorption.

^c Based on the actual Pt content, Pt dispersion and the reaction rate at 140 °C

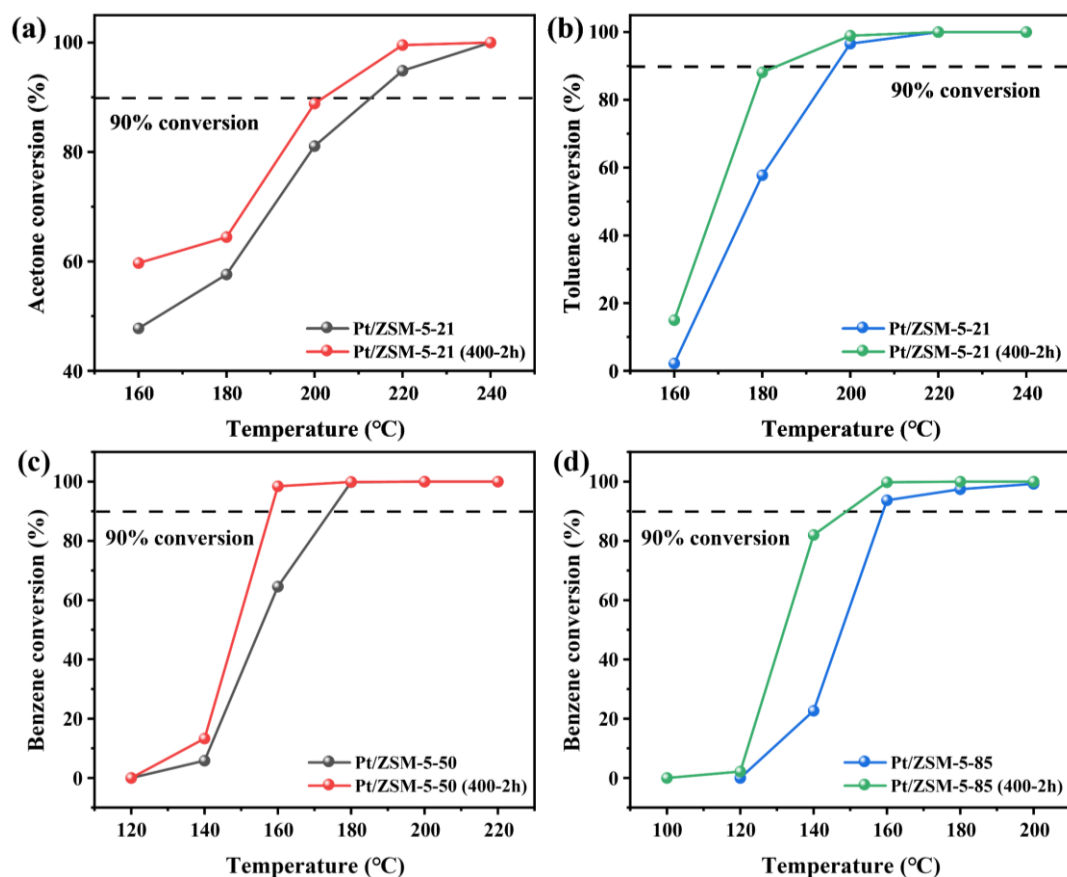


Figure S1 Acetone (a) and toluene (b) conversion curves over Pt/ZSM-5-21 and Pt/ZSM-5-21 (400-2h); benzene conversion curves over Pt/ZSM-5 and Pt/ZSM-5 (400-2h) with (c) 50 or (d) 85 SiO₂/Al₂O₃.

The catalytic activity of toluene and acetone were tested to evaluate the applicability of the hydrothermal strategy. Fig. S1a-b shows that Pt/ZSM-5 (400-2h) possessed higher catalytic activity in both acetone and toluene oxidation than Pt/ZSM-5. This demonstrated that hydrothermal strategy can effectively increase the intrinsic activity for Pt/ZSM-5 rather than just the catalytic activity of benzene oxidation. Encouraged by this, Pt/ZSM-5 with 50 or 85 SiO₂/Al₂O₃ ratio was prepared and hydrothermally treated. Both catalysts showed an enhancement of catalytic activity in benzene oxidation (Fig. S1c-d). This further proved the applicability of this strategy.

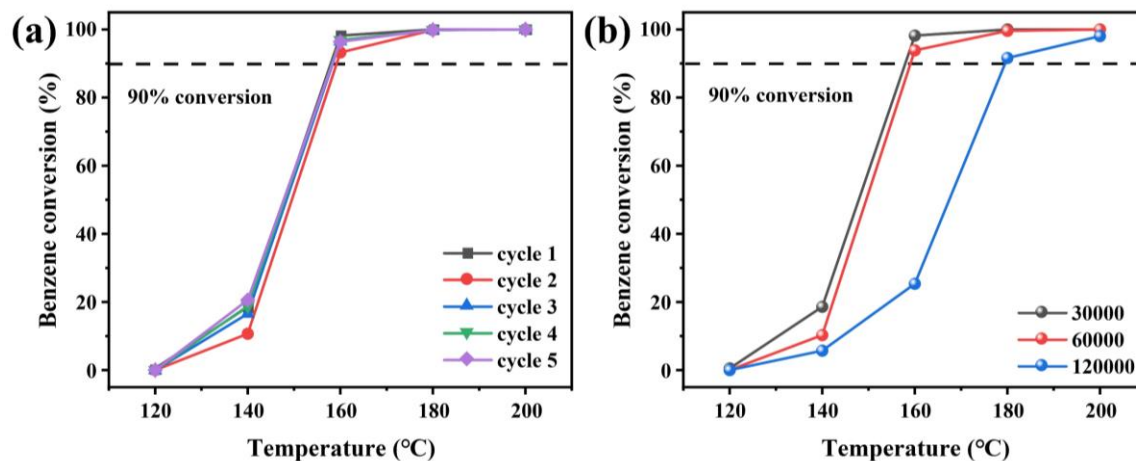


Figure S2 (a) Cycle stability tests over Pt/ZSM-5 (400-2h) catalyst; and (b) effect of WHSV over Pt/ZSM-5 (400-2h) catalyst.

The durability of catalyst is one of the most important indexes for practical applications. In Fig. S2a, no obvious activity loss was observed in 5 repeated benzene oxidation tests, which indicating Pt/ZSM-5 (400-2h) catalyst possessed excellent cycle stability. Besides, the effect of WHSV was also studied. In Fig. S2b, when the WHSV was increased from 30000 mL/(g·h) to 60000 mL/(g·h), there was just a slight decrease in benzene conversion. While, when the WHSV was increased to 120000 mL/(g·h), there was an obvious decrease of benzene conversion. But complete benzene degradation could still be achieved below 200 °C, which demonstrating that Pt/ZSM-5 (400-2h) possessed excellent catalytic performance in high WHSV condition.

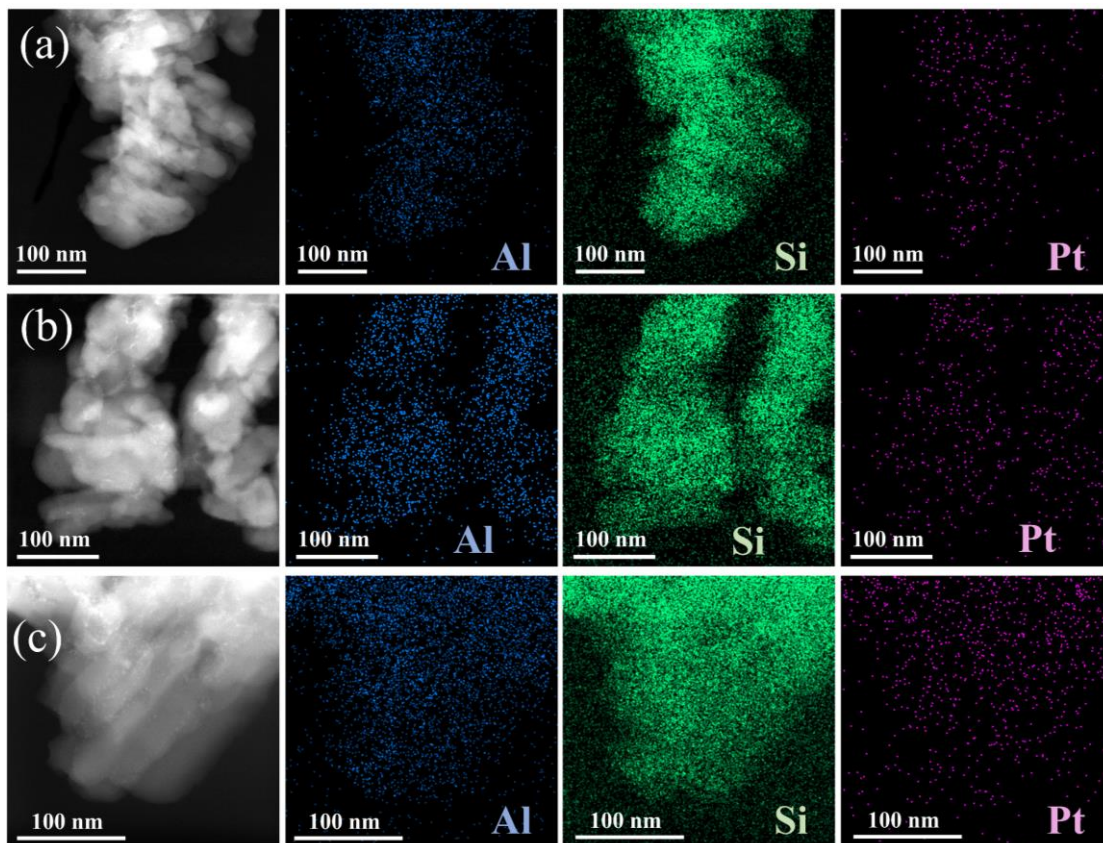


Figure S3 The EDS mapping images of (a) Pt/ZSM-5, (b) Pt/ZSM-5 (100-2h) and (c) Pt/ZSM-5 (400-2h).



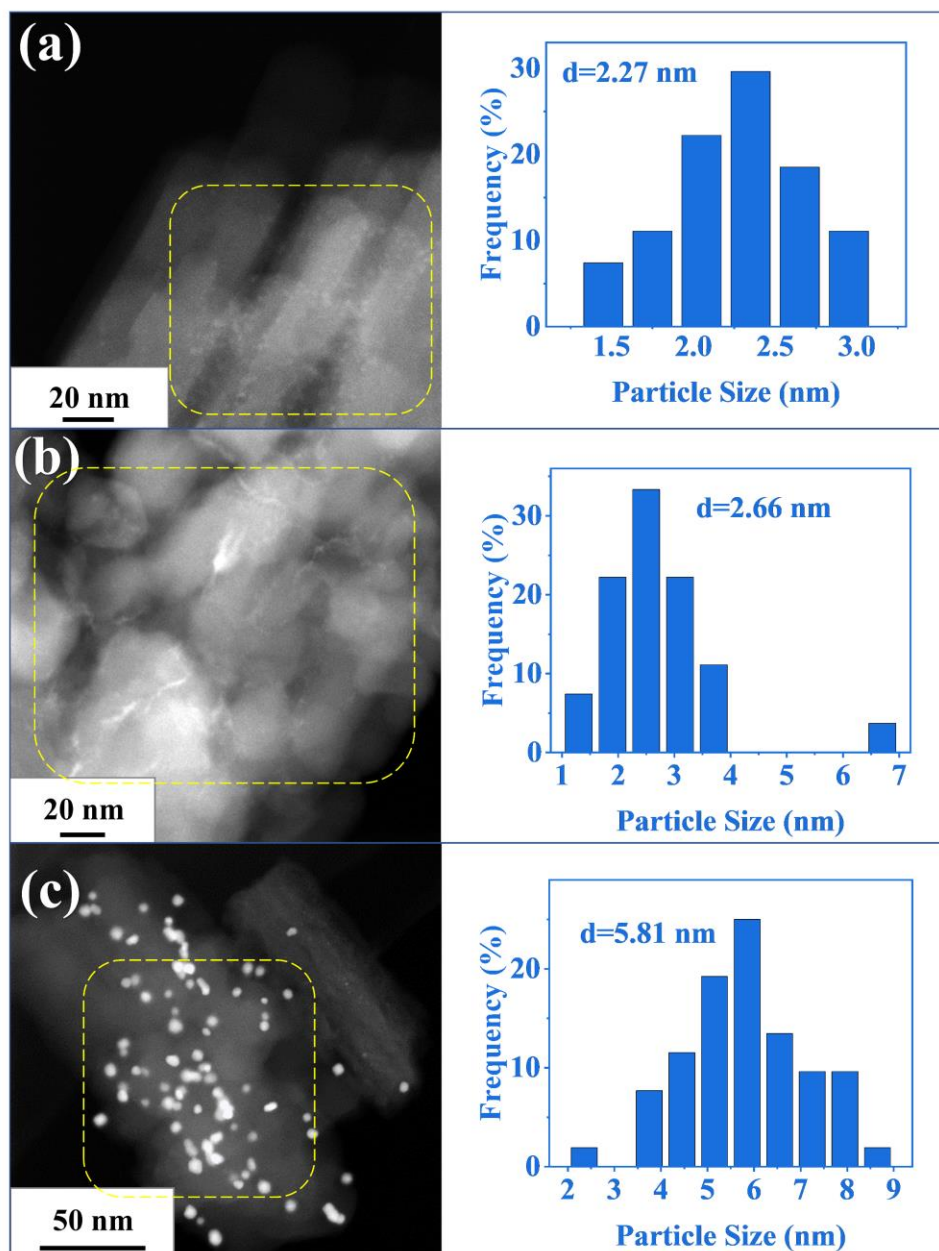


Figure S4 The Pt particle distribution of (a) Pt/ZSM-5, (b) Pt/ZSM-5 (100-2h) and (c) Pt/ZSM-5 (400-2h).

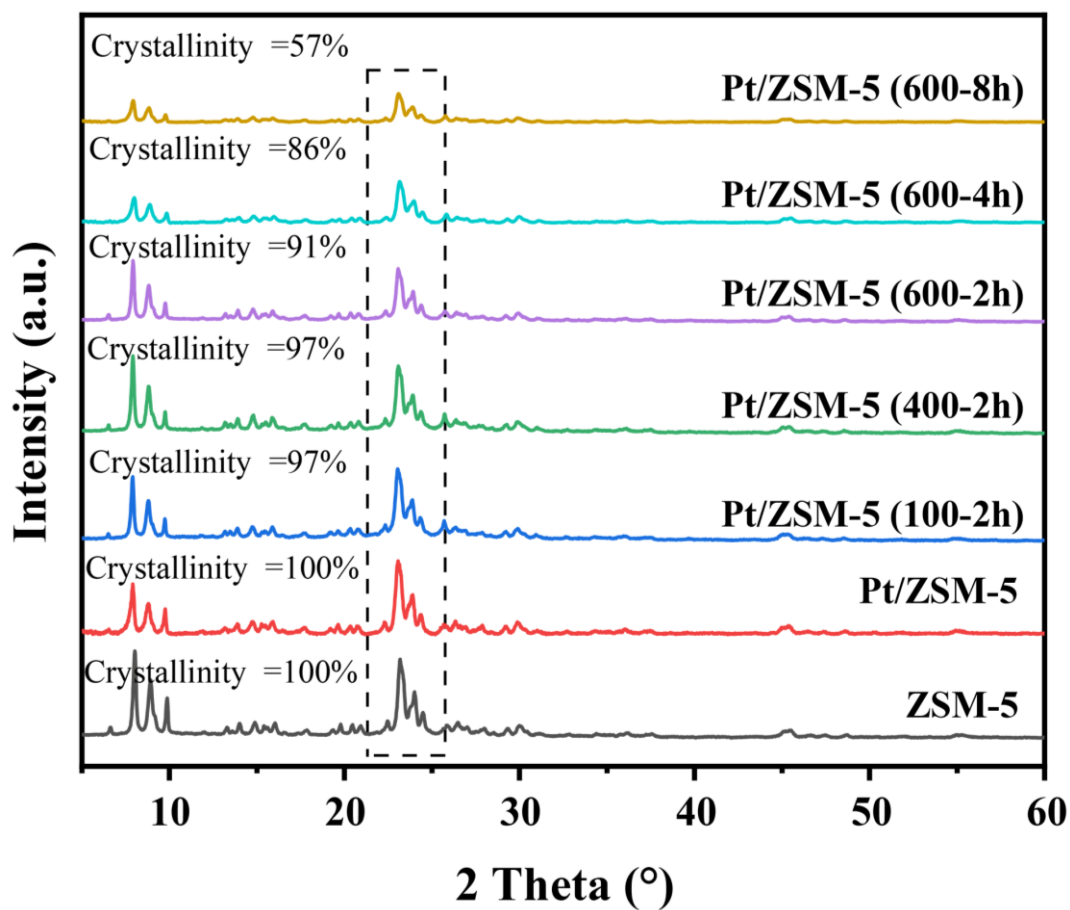


Figure S5 The XRD patterns of ZSM-5, Pt/ZSM-5 and Pt/ZSM-5 with different hydrothermal treatment.

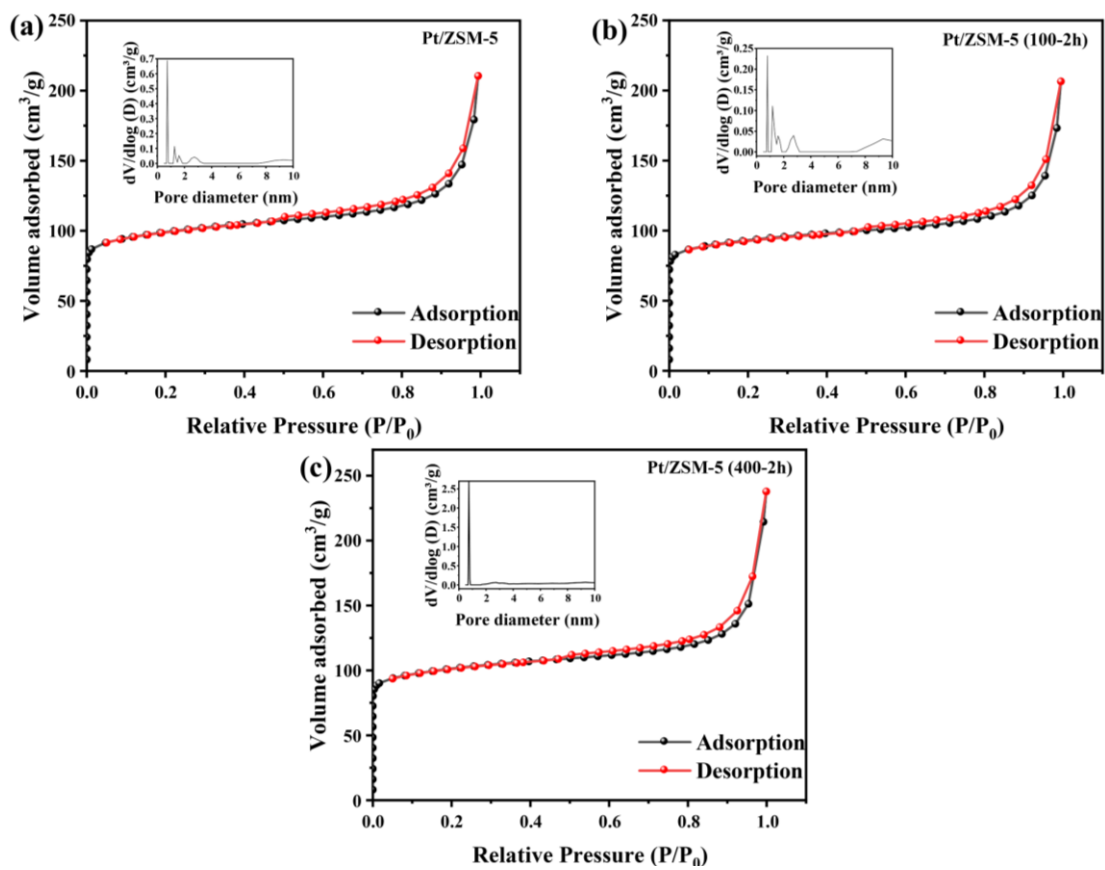


Figure S6 The N_2 adsorption-desorption curve and pore diameter distribution of (a) Pt/ZSM-5, (b) Pt/ZSM-5 (100-2h), and (c) Pt/ZSM-5 (400-2h).

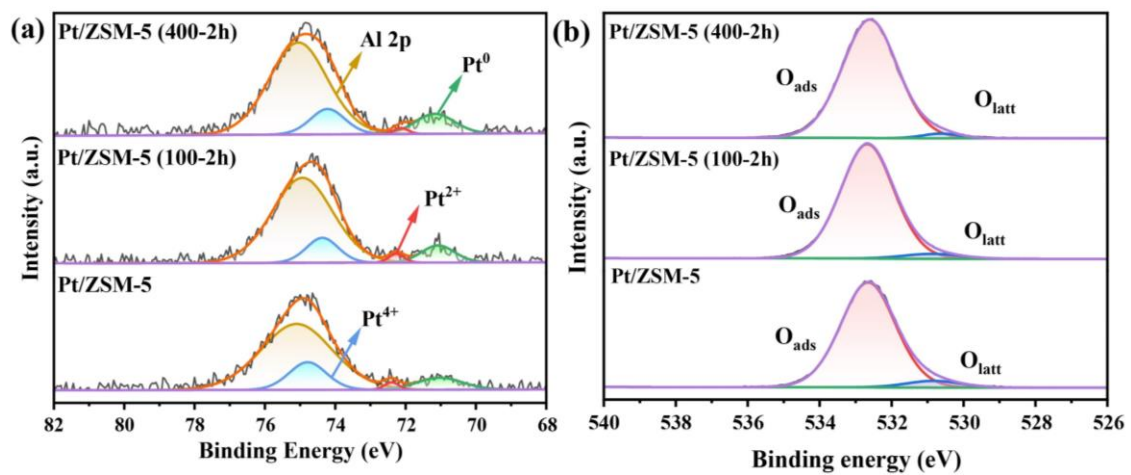


Figure S7 (a) Pt 4f and (b) O 1s XPS spectra of Pt/ZSM-5, Pt/ZSM-5 (100-2h) and Pt/ZSM-5 (400-2h).

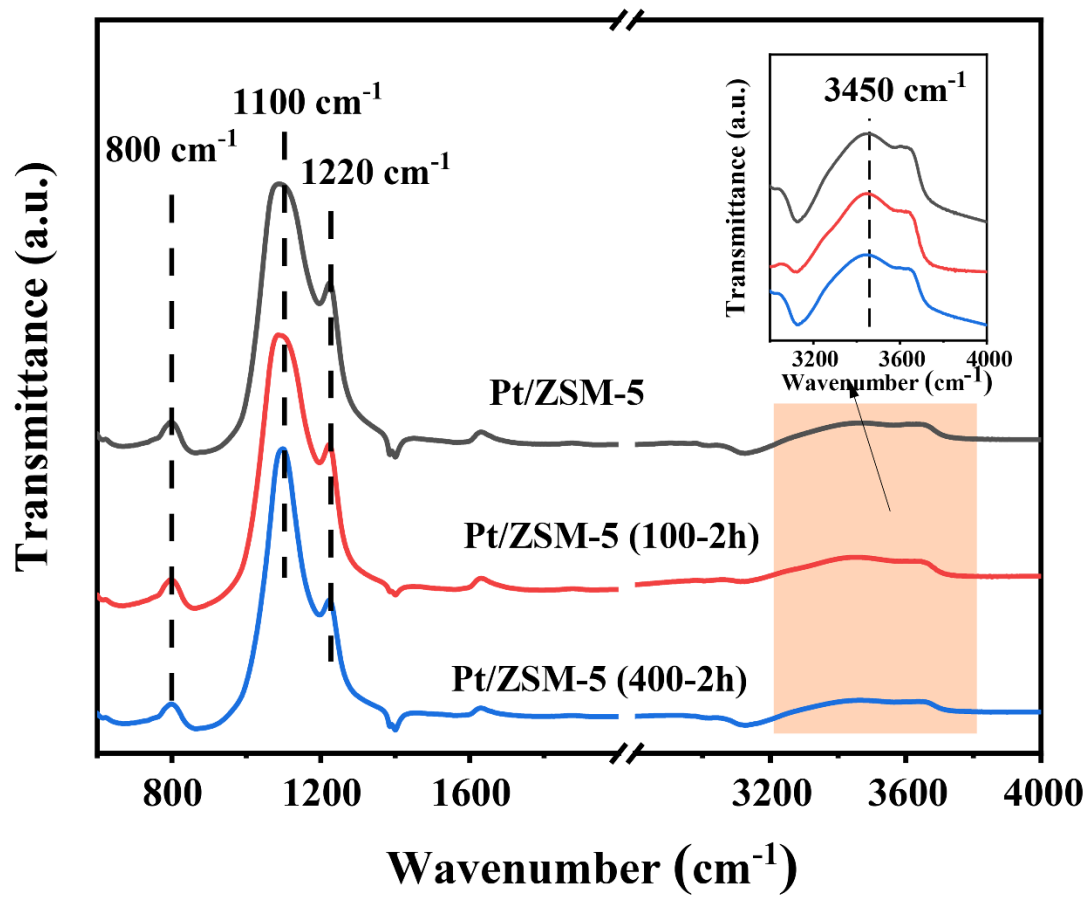


Figure S8 The FT-IR spectrum of Pt/ZSM-5, Pt/ZSM-5 (100-2h) and Pt/ZSM-5 (400-2h).

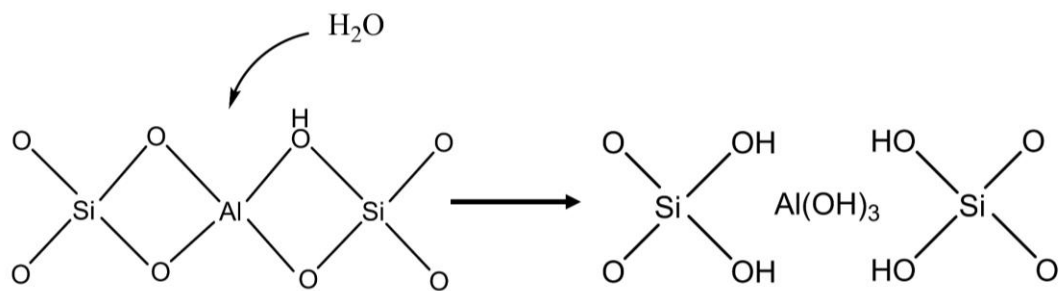


Figure S9 A possible schematic of the destruction of bridging OH groups over Pt/ZSM-5 (400-2h)

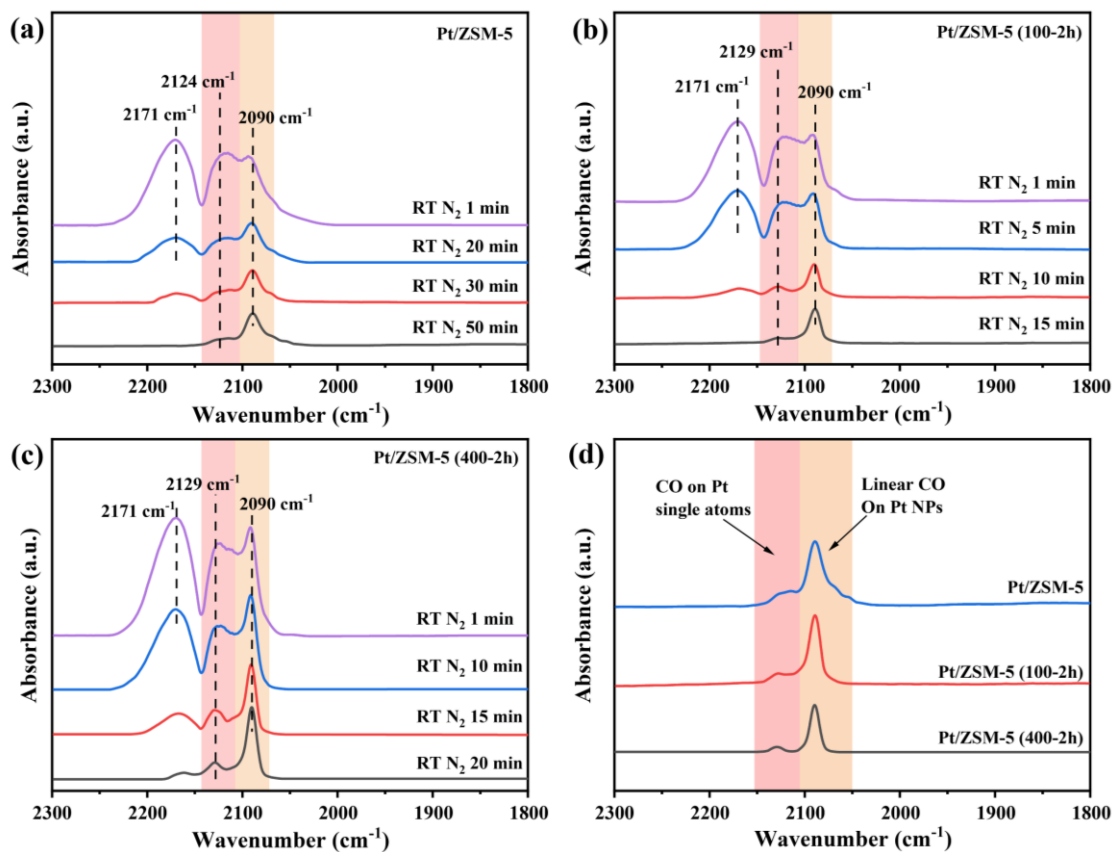


Figure S10 Time-dependent CO DRIFT spectrum of (a) Pt/ZSM-5, (b) Pt/ZSM-5 (100-2h) and (c) Pt/ZSM-5 (400-2h) when purging with N₂; (d) CO DRIFT spectra of Pt/ZSM-5, Pt/ZSM-5 (100-2h) and Pt/ZSM-5 (400-2h) after N₂ purging.

CO DRIFTS was used to study the structure of Pt species on catalyst. As shown in Fig. S8a-c, the band at 2171 cm⁻¹ was assigned to gas phase CO adsorption. The bands at 2124 cm⁻¹ to 2129 cm⁻¹ and 2090 cm⁻¹ were attributed to the linear adsorption of CO on Pt single atoms and nanoparticles, respectively.⁸ This shows the coexistence of Pt single atoms and Pt nanoparticles on Pt/ZSM-5, Pt/ZSM-5 (100-2h) and Pt/ZSM-5 (400-2h). The band at 1860 cm⁻¹ is the bridged CO adsorption on Pt species, and it was not observed on all three catalysts.⁹ The smaller Pt particles was reported to adsorb more CO molecules.¹⁰ Therefore, the integral area of the band is inversely proportional to the Pt particles size. Fig. S8d shows that the band area of

Pt/ZSM-5 (400-2h) was lower than that of Pt/ZSM-5 and Pt/ZSM-5 (100-2h) indicating Pt/ZSM-5 (400-2h) had larger particle size. This was in agreement with STEM results.

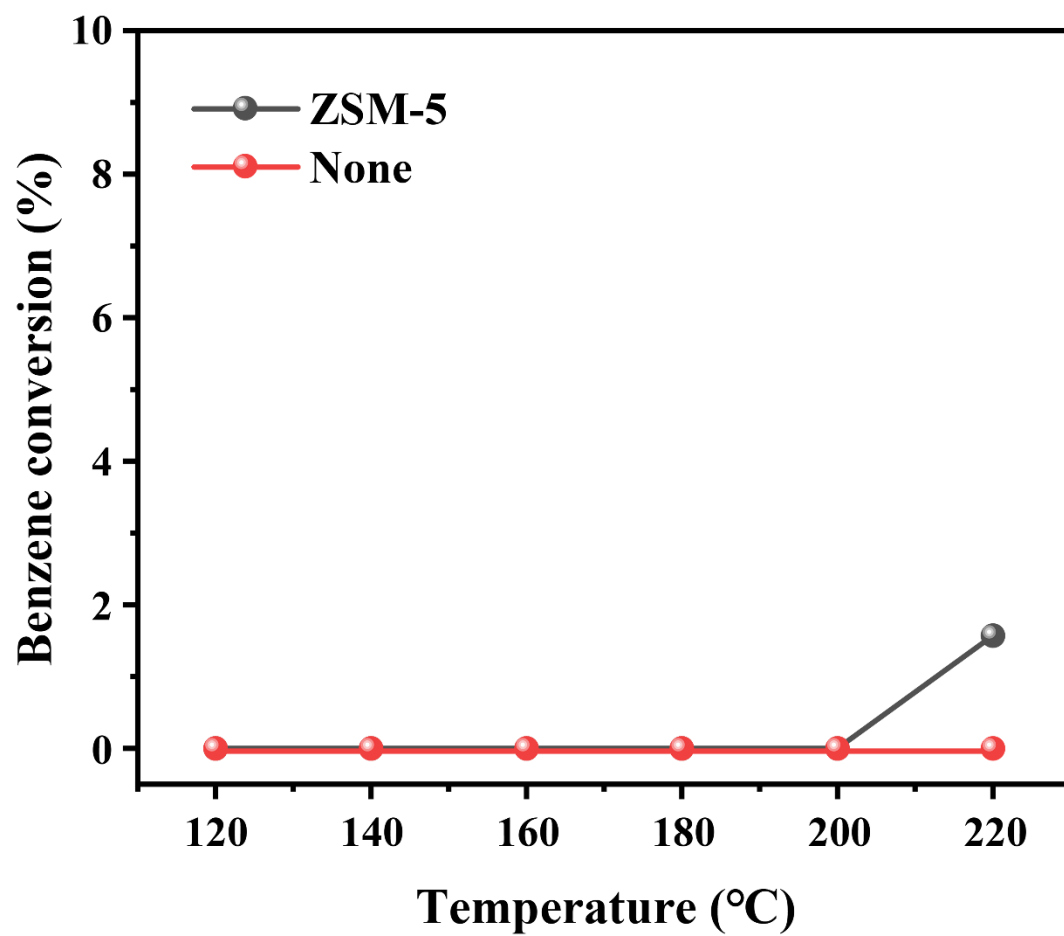


Figure S11 Benzene conversion curves over ZSM-5 and in the absence of catalyst.

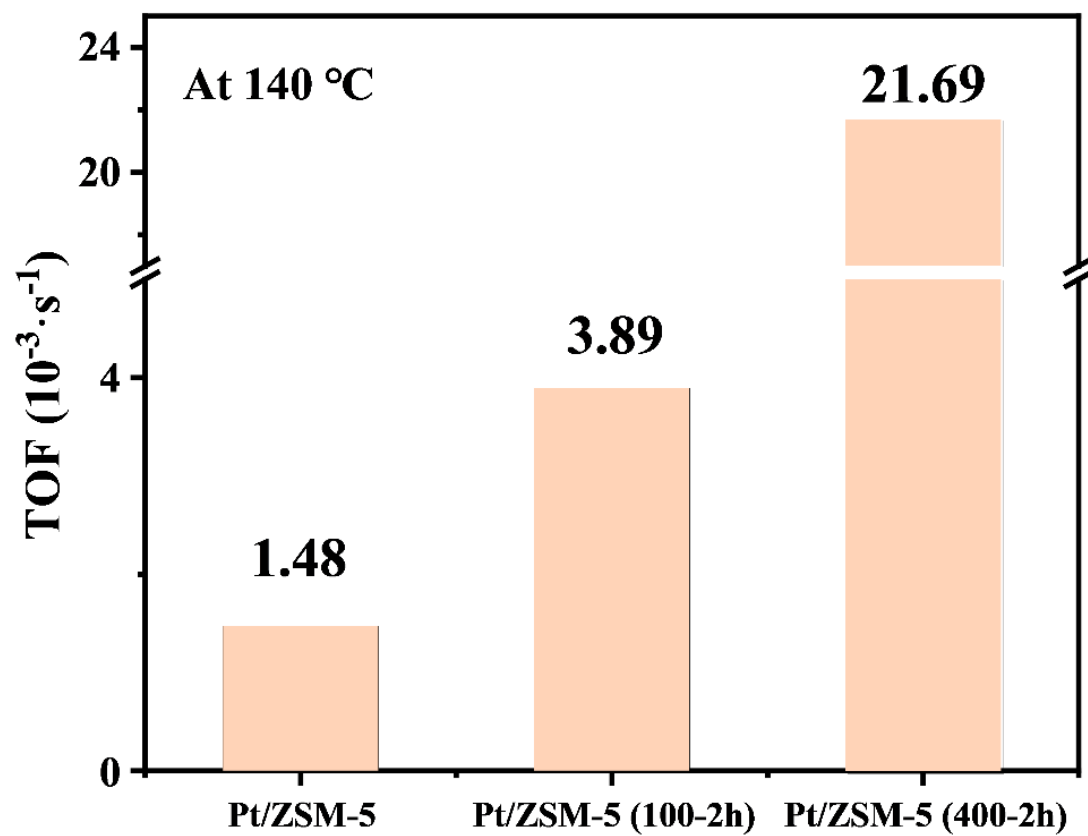


Figure S12 TOF values of Pt/ZSM-5, Pt/ZSM-5 (100-2h) and Pt/ZSM-5 (400-2h) at 140 °C.

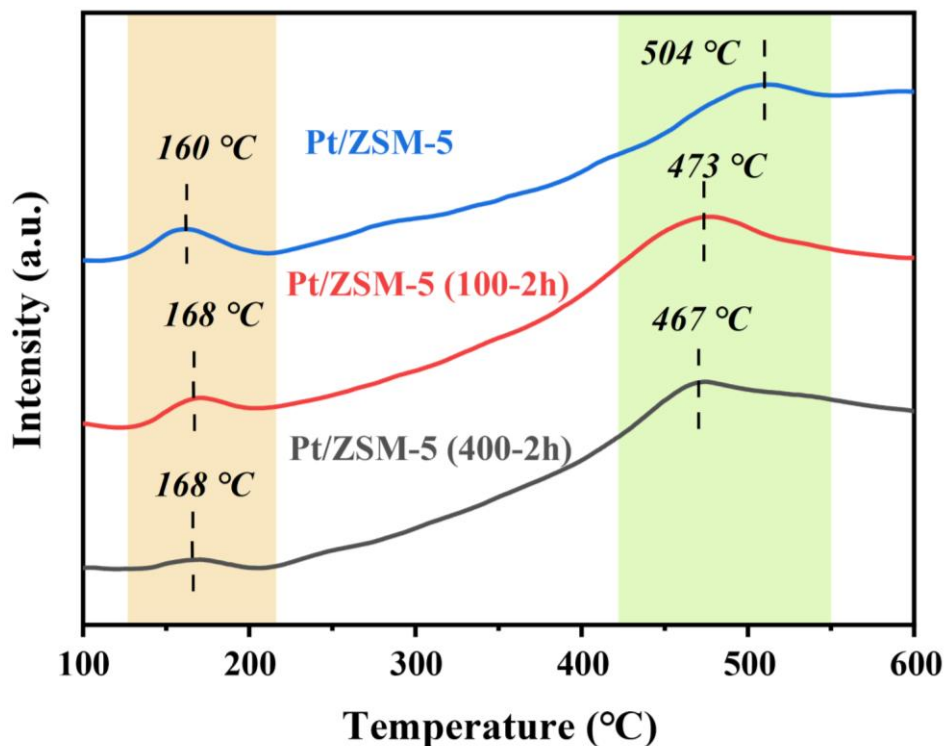


Figure S13 The H₂-TPR patterns of Pt/ZSM-5, Pt/ZSM-5 (100-2h) and Pt/ZSM-5 (400-2h).

The redox properties of catalysts were investigated by H₂-TPR. The peaks centered at 160 °C - 168 °C were attributed to the reduction of PtOx (Fig. S8).¹¹ It can be observed that Pt/ZSM-5 (400-2h) has the smallest reduction peak due to the highest Pt⁰ content. The peaks at 467 °C-507 °C were assigned to the reduction of Pt²⁺ and Pt⁴⁺ species bonded with Si-O in the zeolite.¹² With the treatment temperature increased, the reduction peak shifted toward low temperature, which showed that the catalyst became more reducible.

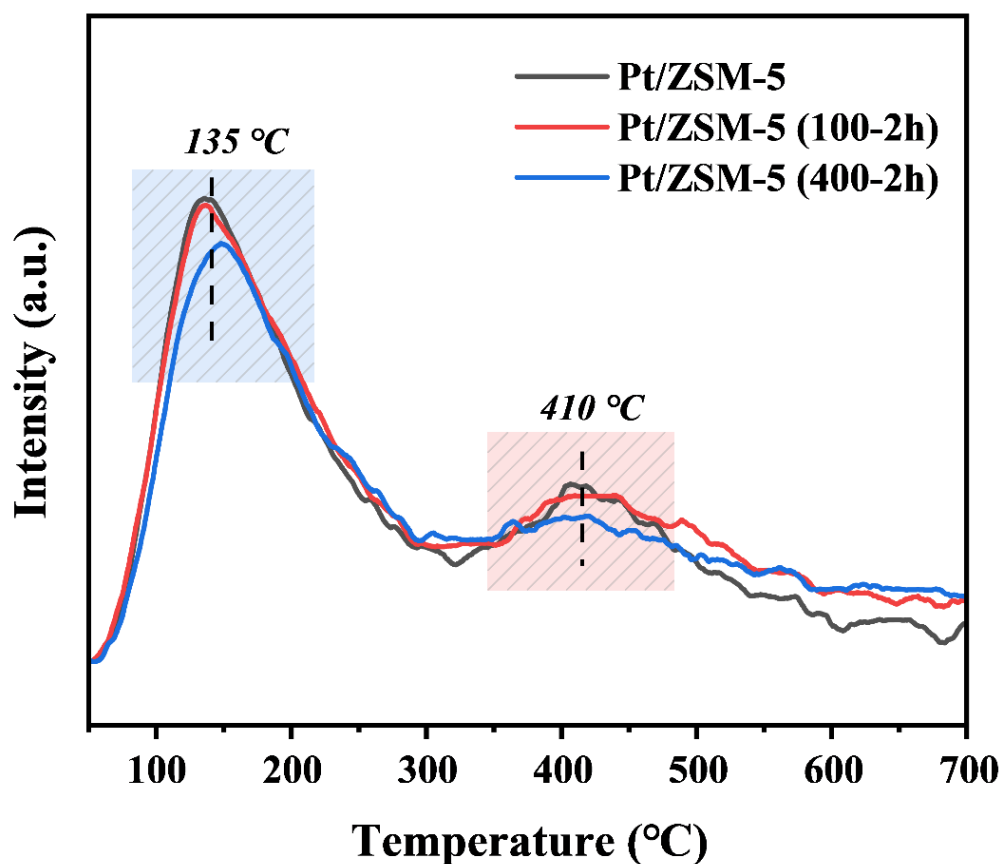


Figure S14 The NH₃-TPD patterns of Pt/ZSM-5, Pt/ZSM-5 (100-2h) and Pt/ZSM-5 (400-2h).

The acidity of catalysts was measured by NH₃-TPD. The peak ranging around 135 °C could be attributed to NH₃ adsorbed on the weak acid sites. While, the peak at 410 °C, was assigned to the NH₃ desorption related to strong acid sites.¹³ As shown in Fig. S11, compare to the other two catalysts, there was an obvious decrease in both weak acid sites and strong acid sites on Pt/ZSM-5 (400-2h). Therefore, the acidity was considered not a key factor affecting the benzene catalytic performance.

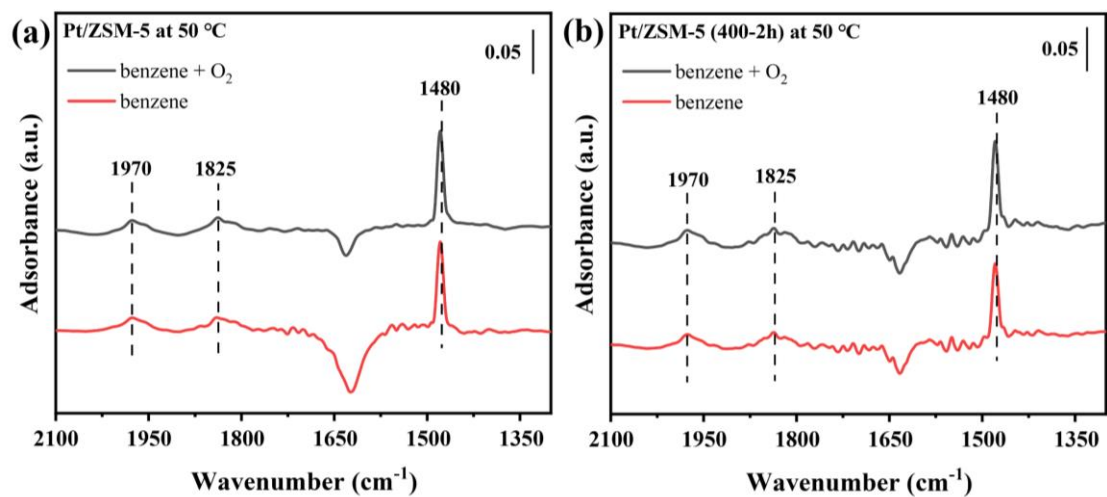


Figure S15 In-situ DRIFT spectrum of benzene adsorption over (a) Pt/ZSM-5 and (b) Pt/ZSM-5 (400-2h) at 50 °C.

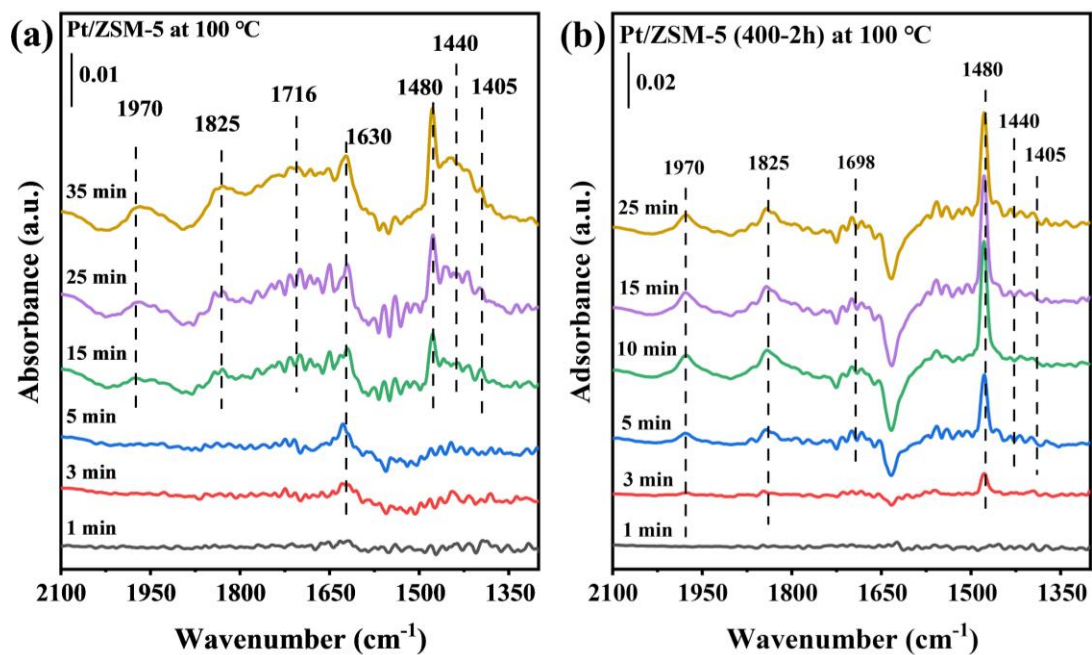


Figure S16 Temperature-dependent in-situ DRIFT spectrum of benzene oxidation over (a) Pt/ZSM-5 and (b) Pt/ZSM-5 (400-2h).

Supplementary references

1. X. Hao, L. Dai, J. Deng, Y. Liu, L. Jing, J. Wang, W. Pei, X. Zhang, Z. Hou and H. Dai, *The Journal of Physical Chemistry C*, 2021, **125**, 17696-17708.
2. K. Zhang, L. Dai, Y. Liu, J. Deng, L. Jing, K. Zhang, Z. Hou, X. Zhang, J. Wang, Y. Feng, Y. Zhang and H. Dai, *Applied Catalysis B: Environmental*, 2020, **279**, 119372.
3. J. Tian, C. Wang, J. Wu, D. Sun and Q. Li, *Chemical Engineering Journal*, 2023, **451**, 138351.
4. B. Wu, B. Chen, X. Zhu, L. Yu and C. Shi, *Catalysis Today*, 2020, **355**, 512-517.
5. J. Tian, K. B. Tan, Y. Liao, D. Sun and Q. Li, *Chemosphere*, 2022, **292**, 133446.
6. P. Yang, J. Li, Z. Cheng and S. Zuo, *Applied Catalysis A: General*, 2017, **542**, 38-46.
7. Y. Shi, J. Wan, F. Kong, Y. Wang and R. Zhou, *Colloids and Surfaces A: Physicochemical and Engineering Aspects*, 2022, **652**, 129932.
8. K. Ding, A. Gulec, A. M. Johnson, N. M. Schweitzer, G. D. Stucky, L. D. Marks and P. C. J. S. Stair, 2015, **350**, 189 - 192.
9. B. Han, Y. Guo, Y. Huang, W. Xi, J. Xu, J. Luo, H. Qi, Y. Ren, X. Liu, B. Qiao and T. Zhang, 2020, **59**, 11824-11829.
10. F. Kong, G. Li, J. Wang, Y. Shi and R. Zhou, *Applied Surface Science*, 2022, **606**, 154888.
11. J. Yang, Y. Huang, H. Qi, C. Zeng, Q. Jiang, Y. Cui, Y. Su, X. Du, X. Pan, X. Liu, W. Li, B. Qiao, A. Wang and T. Zhang, *Nature Communications*, 2022, **13**, 4244.
12. Y. Shi, Z. Li, J. Wang and R. Zhou, *Applied Catalysis B: Environmental*, 2021, **286**, 119936.
13. D. Yang, S. Fu, S. Huang, W. Deng, Y. Wang, L. Guo and T. Ishihara, *Microporous and Mesoporous Materials*, 2020, **296**, 109802.